

Supplementary Materials for  
**Cluster nanoarchitecture and structural diversity of PIEZO1 at rest and during activation in intact cells**

Clement Verkest *et al.*

Corresponding author: Stefan G. Lechner, [s.lechner@uke.de](mailto:s.lechner@uke.de)

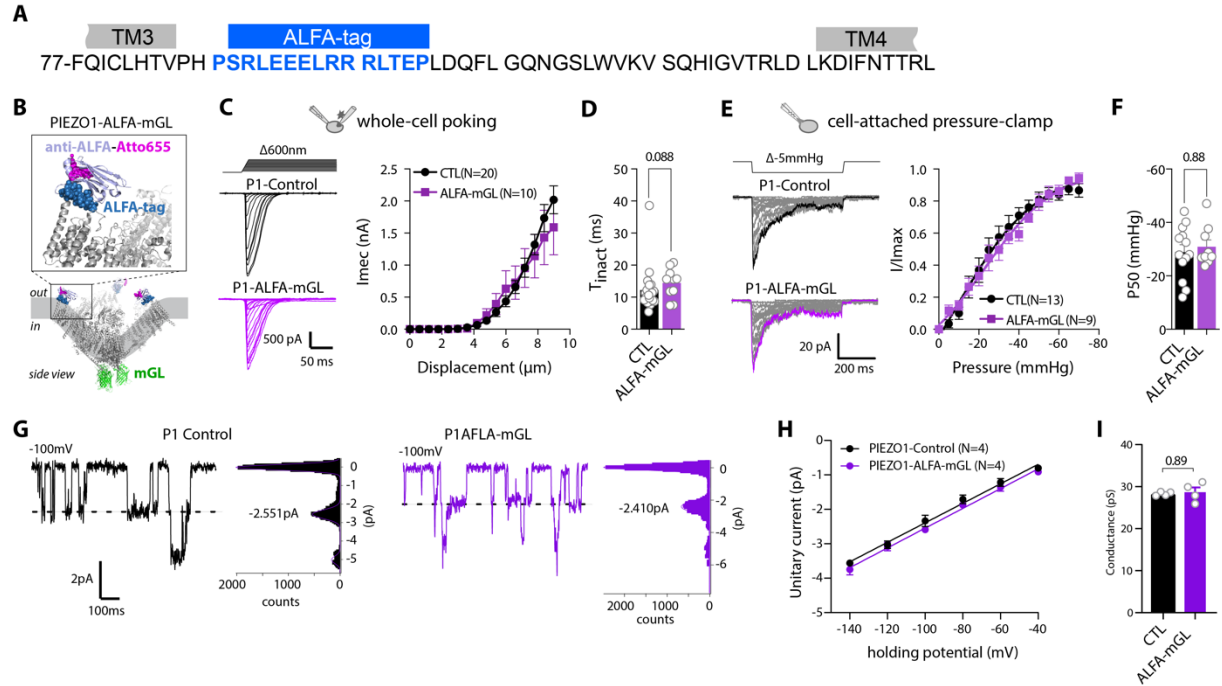
*Sci. Adv.* **11**, eady8052 (2025)  
DOI: 10.1126/sciadv.ady8052

**The PDF file includes:**

Figs. S1 to S11  
Table S1  
Legends for movies S1 to S7

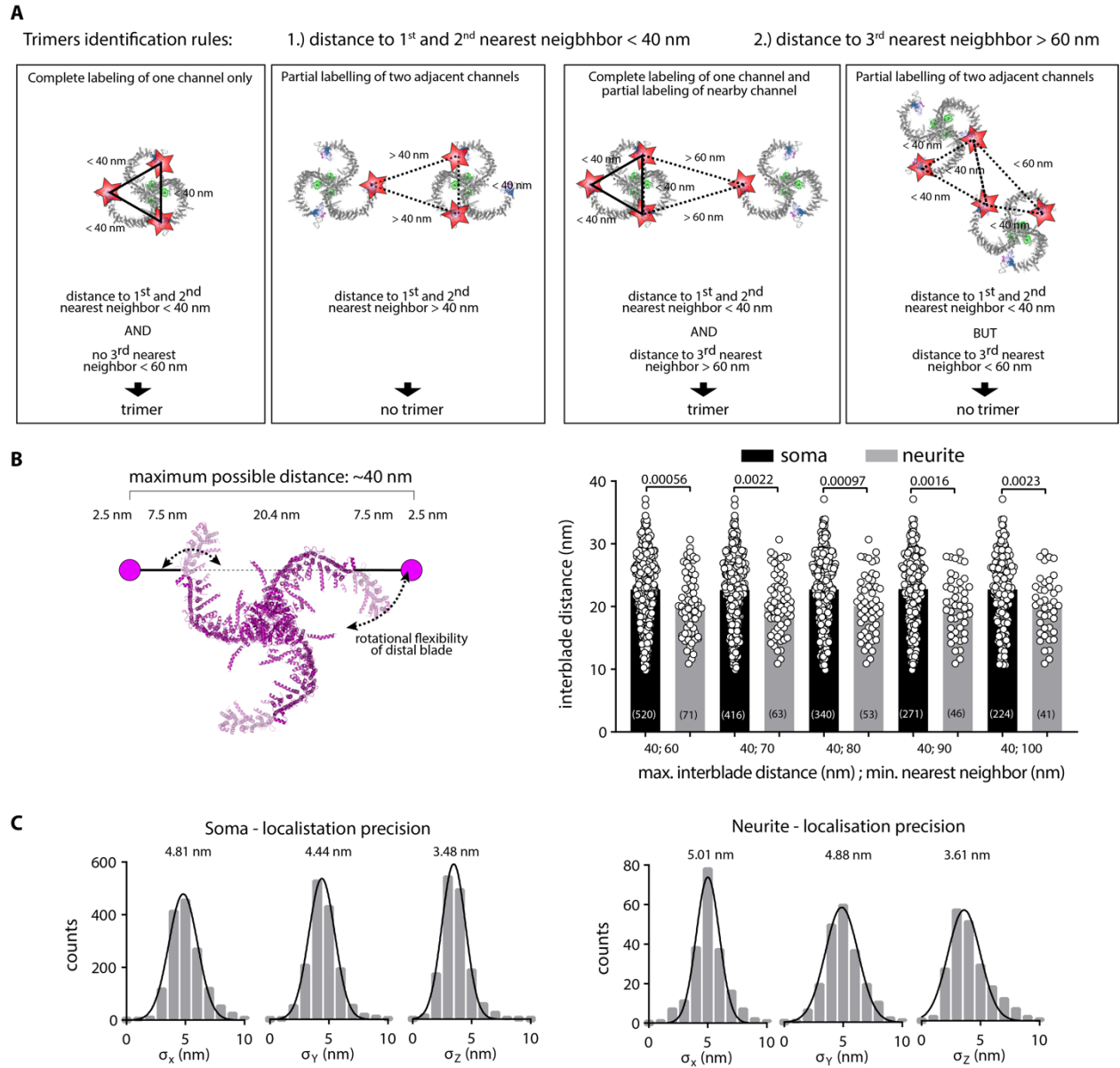
**Other Supplementary Material for this manuscript includes the following:**

Movies S1 to S7

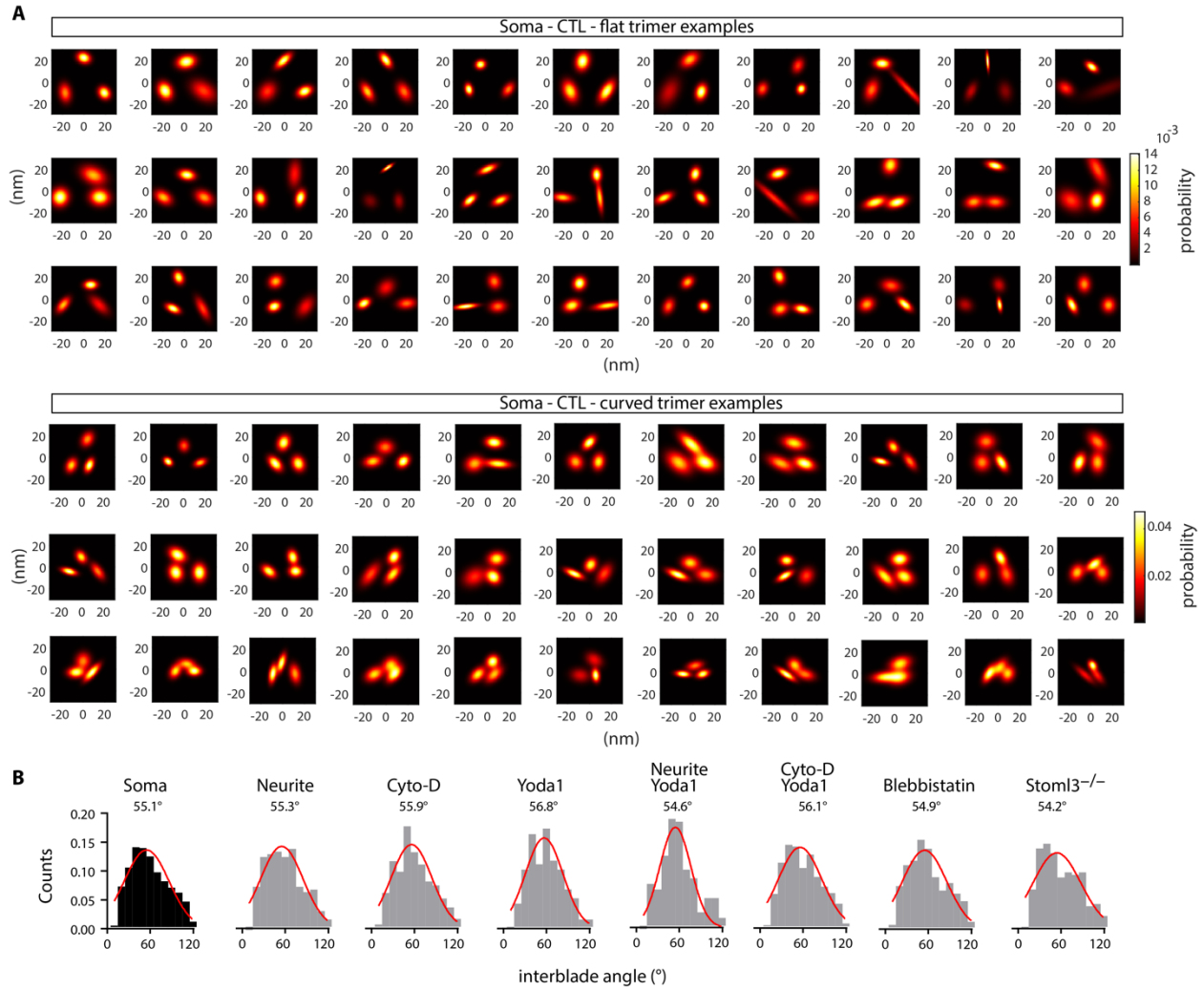


**Supplementary Figure 1, Functional characterization of PIEZO1-ALFA-mGreenLantern.** (A) Amino acid sequence of PIEZO1 indicating the position of the inserted ALFA-tag. (B) Cartoon depicting the position of the extracellular ALFA-tag and intracellular mGL in PIEZO1-ALFA-mGL. (C) Example traces (left) of poking-evoked whole-cell currents of the indicated channel variants (PIEZO1-IRES-GFP, Control, top and PIEZO1-ALFA-mGreenLantern, bottom) in N2a-P1KO and displacement-response curve of mean  $\pm$  s.e.m. peak current amplitudes (right). (D) Comparison of the mean  $\pm$  s.e.m. of the inactivation time constants of PIEZO1 currents using two-tailed Mann-Whitney. (E) Representative traces (left) of stretch-evoked cell-attached currents and normalized pressure-response curve of mean  $\pm$  s.e.m. peak current amplitudes ( $I/I_{\text{max}}$ ) of PIEZO1-Control and PIEZO1-ALFA-mGL. (F) Comparison of the mean  $\pm$  s.e.m. P50 values with two-tailed unpaired t-test. (G) Example traces of stretch-evoked single channel openings (left) and corresponding all-points histogram (right), with Gaussian fits and indicated peak average of PIEZO1-IRES-GFP (Control) and PIEZO1-ALFA-mGL. (H) Relation between mean  $\pm$  s.e.m. single-channel amplitudes and holding potential fitted with a linear regression. (I) Comparison of the mean  $\pm$  s.e.m. single-channel conductance with Mann Whitney test.

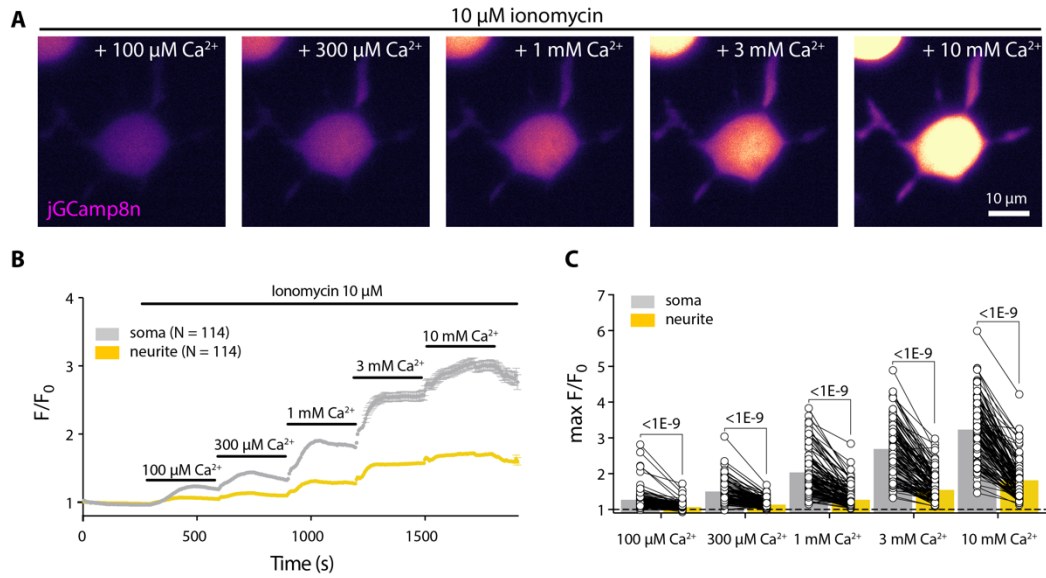




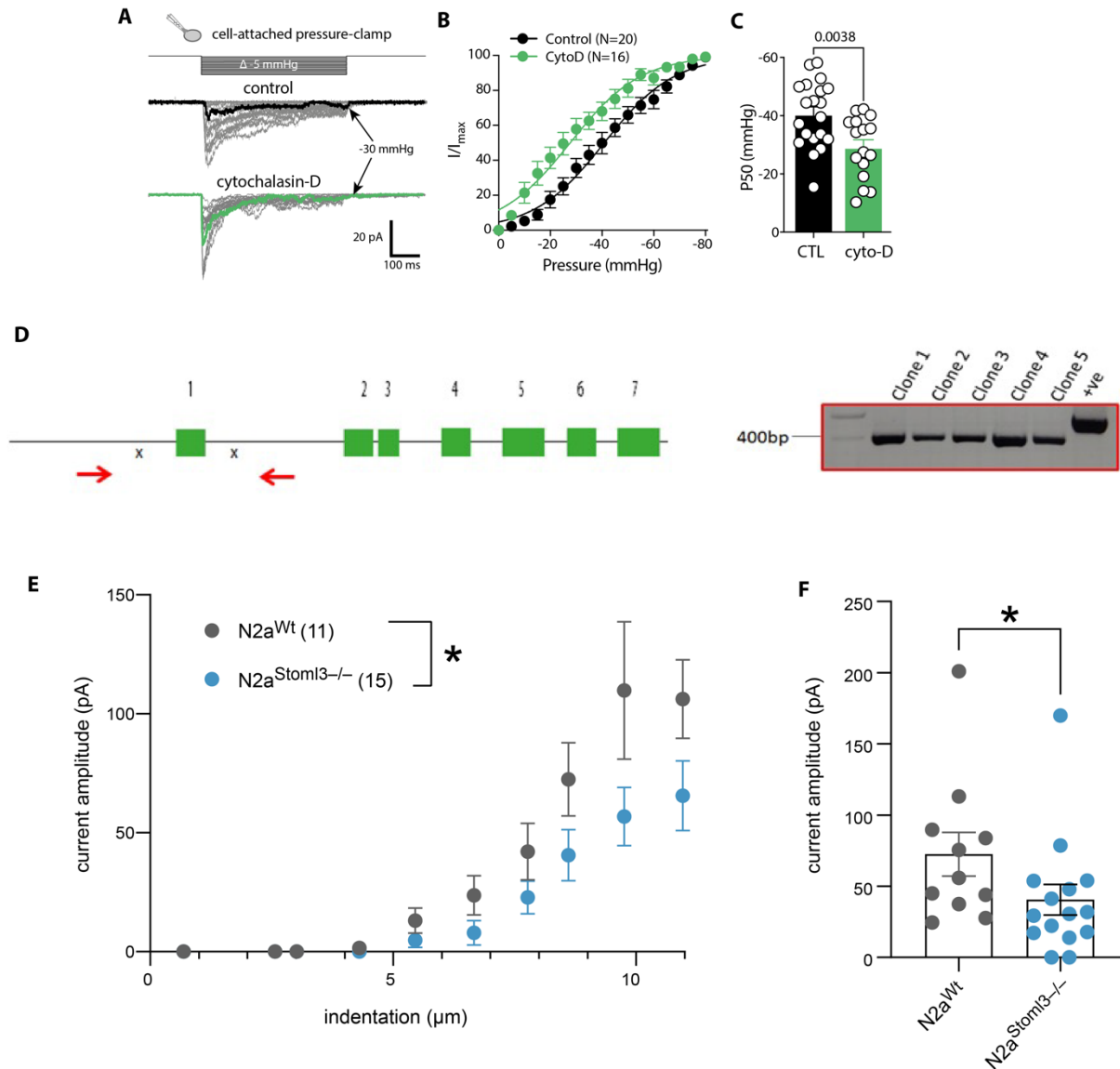
**Supplementary Figure 3, PIEZO1-ALFA-mGreenLantern trimer identification.** (A) Overview of the PIEZO1 trimers identifications rules from MINFLUX ALFA signals. (B) Schematic representation of a full length flattened PIEZO1 structure (left), illustrating the maximum measurable interblade distance when taking into account peripheral blade flexibility and linkage error. Bar graphs (right) of the mean interblade distance between soma- and neurite-localized PIEZO1 trimers detected with different cutoffs for trimer identification: maximum interblade distance of 40nm and varying minimum nearest neighbour distance. Comparison with Mann Whitney-tests. (C) Distribution of the standard deviations along the x, y, and z-axis of the MINFLUX traces making soma (left) or neurite (right) identified PIEZO1 trimers.



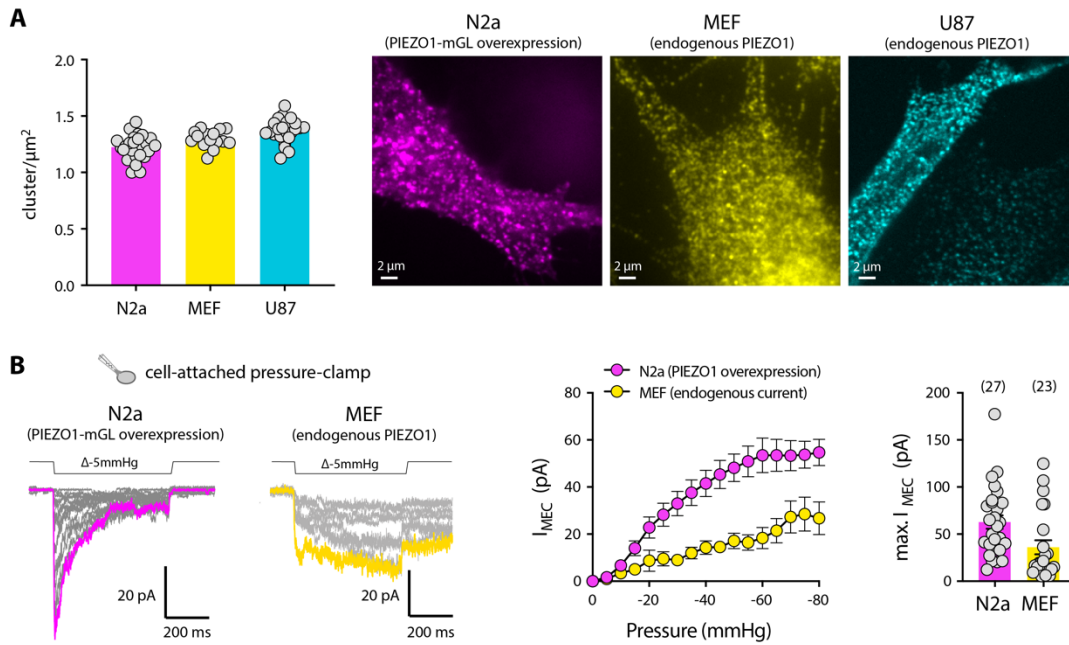
**Supplementary Figure 4, Examples of different class of MINFLUX-identified PIEZO1 trimers in control cell soma. (A)** Representative examples of 33 PIEZO1-ALFA-mGL trimers identified in the soma and for each of the three classes: flat, curved and supercurved. Trimers are displayed as 2D-projection of the probability density of the raw localizations making each protomer. **(B)** Histogram of all the measured interblade angle for soma- (black), neurite, cyto-D, Yoda1, neurite plus Yoda1, cyto-D plus Yoda1, blebbistatin and SLP3-KO (gray) PIEZO1 trimers. Gaussian fit (red or black line) and average are indicated on the graph.



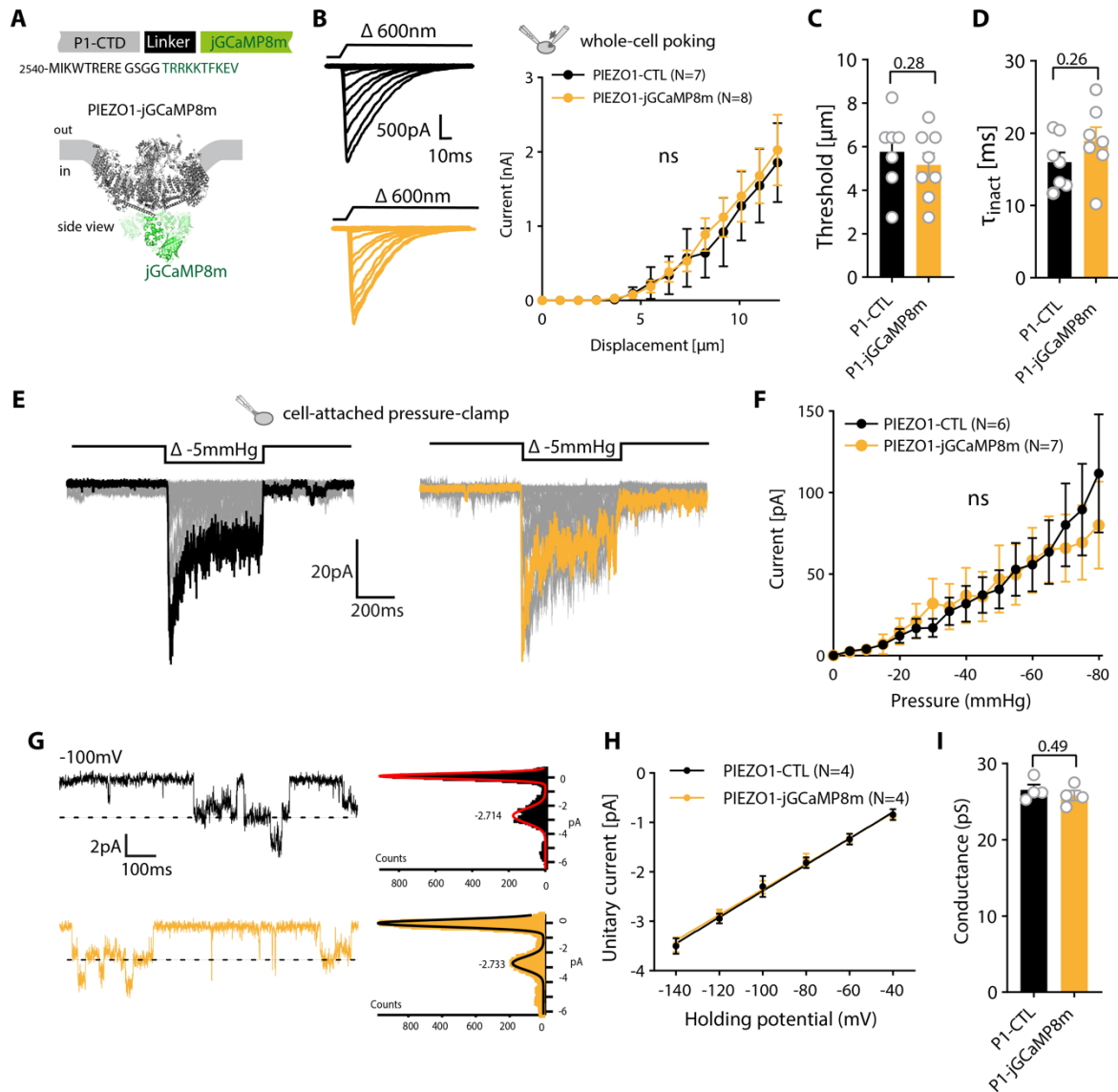
**Supplementary Figure 5, Neurites response to ionomycin.** (A) Example images of a N2A-P1KO cell transfected with jGCaMP8m, exposed to 10 $\mu\text{M}$  ionomycin with increasing concentration of calcium. (B) Time-course of the normalized fluorescence ( $F/F_0$ ) of N2A-P1KO cells and their neurites. (C) Comparison of the max  $F/F_0$  determined for each concentration between cell soma and their neurite, with paired t-test.



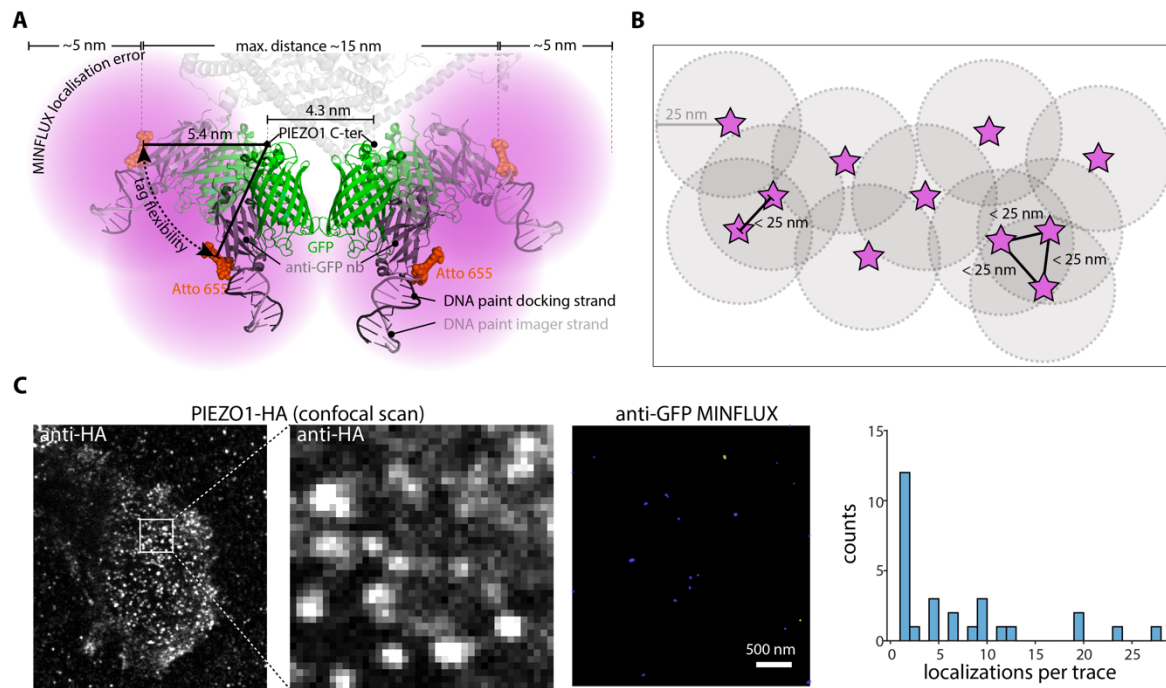
**Supplementary Figure 6, Effect of cytoskeletal disruption by cyto-D on PIEZO1 cell-attached currents.** (A) Example traces of PIEZO1-mediated currents evoked by negative pressure in cell attached patch-clamp recordings with or without cyto-D. (B) Normalized ( $I/I_{max}$ ) pressure-response curves of PIEZO1 currents recorded from control (black circles) and cyto-D treated (green circles) cells. (C) Comparison of the mean  $\pm$  sem P50 values, using Student's t-test (CTL:  $p50 = -40.6 \pm 2.5$  mmHg, N=20 vs. cyto-D:  $p50 = -29.1 \pm 2.6$  mmHg, N=16;  $P = 0.0038$ ). White circles show values from individual cells. (D), Schematic showing experimental strategy for knocking out *Stoml3* by deletion of exon 1 (left) in *N2a* cells and gel showing reduced size of DNA fragments amplified from the targeted regions from five selected clones (right). (E) Current amplitudes evoked in  $N2A^{wt}$  and  $N2A^{Stoml3-/-}$  cells with a series of indentation stimuli of increasing amplitude. Note that current amplitudes were significantly reduced in  $N2A^{Stoml3-/-}$  cells compared to  $N2A^{wt}$  cells ANOVA analysis  $P=0.0491$  ( $F(1, 24) = 4.296$ ). (F) Current amplitudes measured with stimuli of  $8\mu m$  were also significantly lower in  $N2A^{Stoml3-/-}$  cells compared to  $N2A^{wt}$  cells (Mann Whitney U test  $P=0.03$ ).



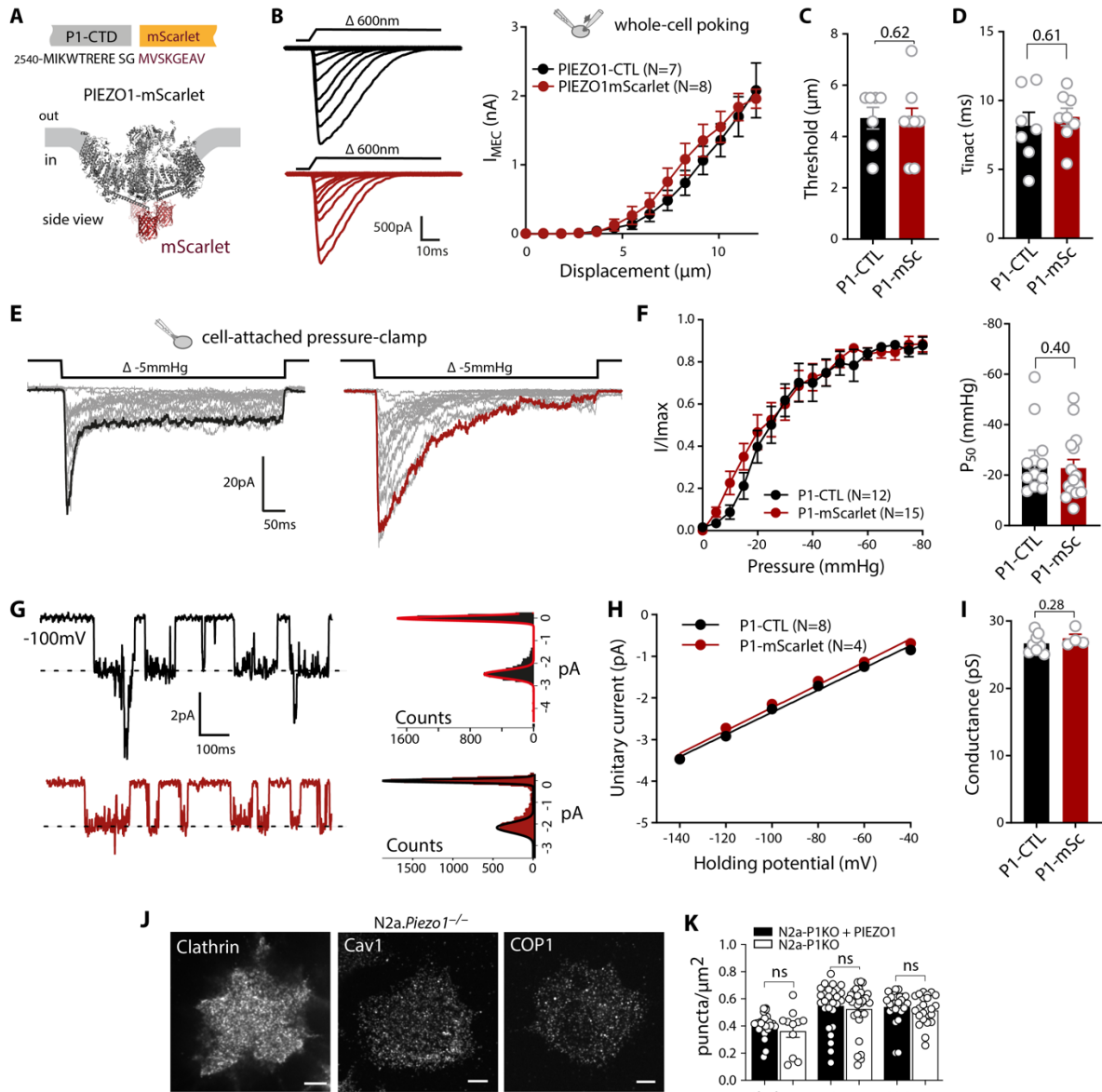
**Supplementary Figure 7, Additional characterization of endogenous and recombinant PIEZO1 clusters.** (A) Quantification (left) of the number of PIEZO1 clusters detected in N2A-P1KO cells expressing PIEZO1-mGL and in MEF and U87 cells (endogenous expression). Additional representative images of N2A-P1KO cells expressing PIEZO1-mGL and MEF and U87 labelled with anti-PIEZO1 antibody (right). (B) Representative traces (left) from cell-attach pressure clamp recording of N2A-P1KO cells expressing PIEZO1-mGL and from endogenous PIEZO1 in MEF cells. Pressure-response curve of mean peak current amplitudes in N2A-P1KO plus PIEZO1-mGL and in MEF, with a comparison of the maximum current per cell (right).



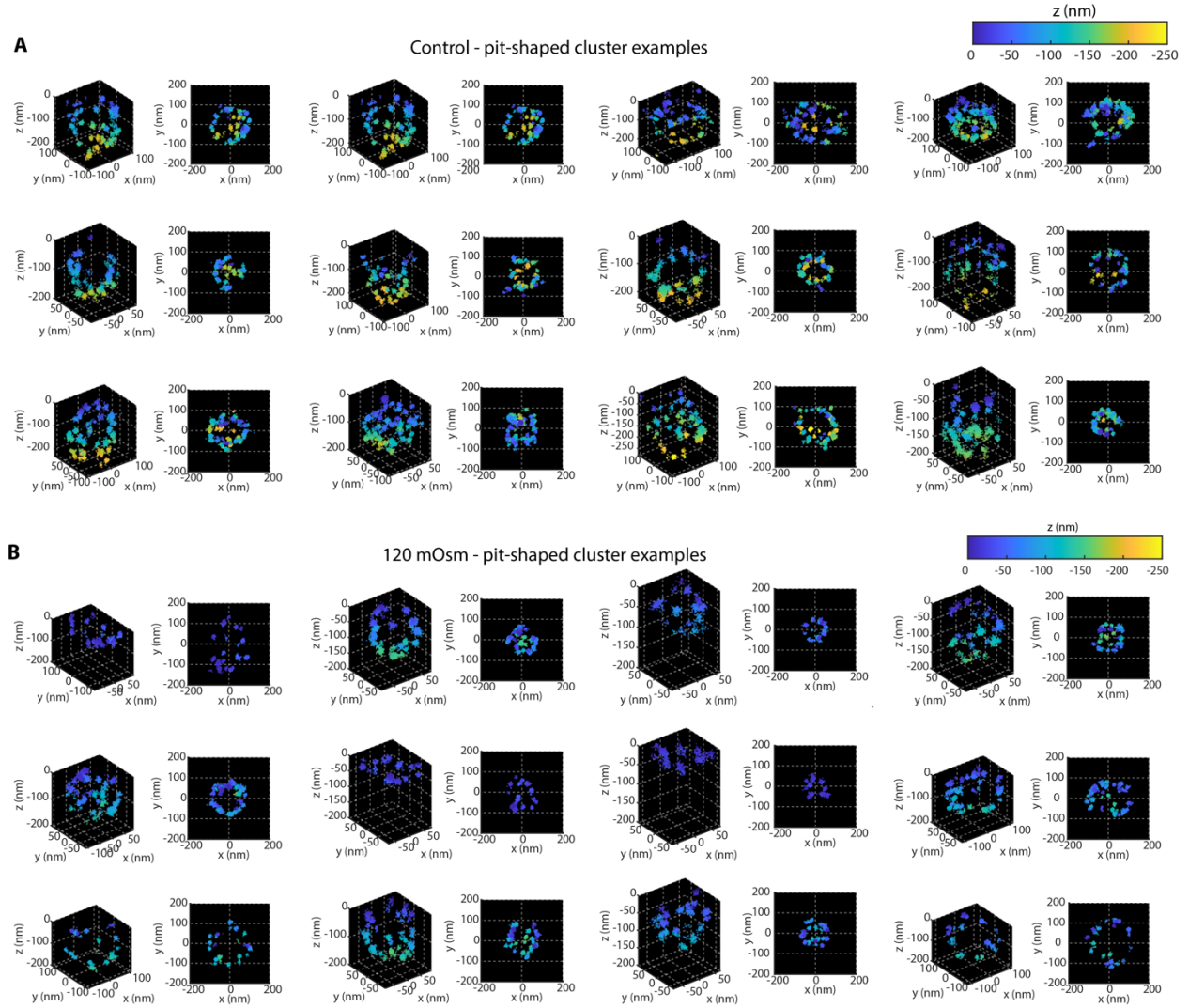
**Supplementary Figure 8, Functional characterization of PIEZO1-jGCaMP8m.** (A) Amino-acid sequence of the inserted jGCaMP8m (top) and its putative location at PIEZO1 C-ter structure (PDB 7st4). (B) Example traces (left) of poking-evoked whole-cell currents of the indicated channel variants (PIEZO1-IRES-GFP, top and PIEZO1-jGCaMP8m, bottom). Displacement-response curve (right) of mean peak current amplitudes. (C) Comparison of the mean mechanical thresholds using Mann-Whitney test. (D) Comparison of the mean of the inactivation time constants of PIEZO1 currents using Mann-Whitney test. (E) Representative traces of stretch-evoked cell-attached currents from PIEZO1-Control (left) and PIEZO1-jGCaMP8m (right). (F) Pressure-response curve of mean peak current amplitudes of PIEZO1-Control and PIEZO1-jGCaMP8m. (G) Example traces of stretch-evoked single channel openings (left) and corresponding all-points histogram (right), with Gaussian fits. (H) Relation between mean single-channel amplitudes and holding potential, fitted with a linear regression. (I) Comparison of the mean single-channel conductance with Mann-Whitney test.



**Supplementary Figure 9, 3D MINFLUX acquisition and processing pipeline of PIEZO1mGreenLantern data.** (A) Cartoon showing the extend and the sources of linkage error of PIEZO1-mGL/GFP MINFLUX recording. (B) Assignment rules for GFP MINFLUX signals to individual PIEZO channel. (C) Selectivity of the GFP nanobody and MINFLUX signals. Representative confocal scan of PIEZO1-ALFA-HA in N2a-P1KO cell (left), labelled with the anti-GFP nanobody used for MINFLUX DNA-PAINT together with an anti-HA antibody for cluster visualization, with a closeup of the selected region for MINFLUX scan (middle, 3x3µm). Samples were imaged with 1nM of GFP-nb corresponding imager conjugated to Atto655. Raw MINFLUX localizations are depicted (right), together with the corresponding histogram of the number of localizations per trace.



**Supplementary Figure 10, Functional characterization of PIEZO1-mScarlet.** (A) Amino-acid sequence of the inserted mScarlet (top) and its putative location at PIEZO1 C-ter structure (PDB 5lk4). (B) Example traces (left) of poking-evoked whole-cell currents of the indicated channel variants (PIEZO1-IRES-GFP, top and PIEZO1-mScarlet, bottom). Displacement-response curve (right) of mean peak current amplitudes. (C) Comparison of the mean mechanical thresholds using Mann-Whitney test. (D) Comparison of the mean of the inactivation time constants of PIEZO1 currents using Mann-Whitney test. (E) Representative traces of stretch-evoked cell-attached currents from PIEZO1-Control (left) and PIEZO1-mScarlet (right). (F) Pressure-response curve of normalized mean peak current amplitudes ( $I/I_{\text{max}}$ ) of PIEZO1-Control and PIEZO1-mScarlet (left). Bar graph of mean  $P_{50}$  (right). Comparison with Mann-Whitney test. (G) Example traces of stretch-evoked single channel openings (left) and corresponding all-points histogram (right), with Gaussian fits. (H) Relation between mean single-channel amplitudes and holding potential, fitted with a linear regression. (I) Comparison of the mean single-channel conductance with Mann-Whitney test. (J) TIRF images of N2a-P1KO cells without recombinant expression of PIEZO1, showing clathrin coated pits (transient expression of Clathrin light chain-mGL), caveolae (Cav19 and COP1-coated vesicles). (K), Comparison of the densities of the indicated invagination in the presence (black) and absence (white) of PIEZO1.



**Supplementary Figure 11, Examples of control and osmotically-challenged pit-shaped PIEZO1 cluster. (A)** Representative examples of 12 control PIEZO1 pit-shaped clusters. MINFLUX raw localizations making the cluster are depicted in a 3D view (left), alongside a z-projected view (right). Localizations are colored based on the relative z position to the top of the cluster. **(B)** Representative examples of 12 pit-shaped osmotically activated PIEZO1 clusters.

Iteration	Modality	Pattern diameter (nm)	photon limit	back-ground limit	dwel time (ms)	pattern repeat	Stickiness	CFR limit	laser power factor
0	hexagonal	251	160	15000	1	1	-	none	1
1	zline	251	400	15000	1	1	2	none	1
2	square	251	100	10000	1	5	2	none	1
3	zline2	251	50	10000	1	5	2	none	1
4	square	132	67	10000	1	5	2	0.9	2
5	zline2	132	33	10000	1	5	2	none	2
6	square	66	67	10000	1	5	2	0.8	4
7	zline2	66	33	10000	1	5	2	none	4
8	square	35	100	10000	1	5	2	none	6
9	zline2	35	50	10000	1	5	2	none	6

**Table S1. 3D-MINFLUX scan parameters**

**Movie S1.** jGCamp8 calcium imaging of PIEZO1 clusters

**Movie S2.** 3D MINFLUX example with raw localizations of a GFP-labelled pit-shape PIEZO1 cluster

**Movie S3.** 3D MINFLUX example with raw localizations of a GFP-labelled spherical PIEZO1 cluster

**Movie S4.** 3D MINFLUX example with raw localizations and surface fit of a GFP-labelled pit-shape PIEZO1 cluster in control condition

**Movie S5.** 3D MINFLUX example with raw localizations and surface fit of a GFP-labelled pit-shape PIEZO1 cluster in hypo-osmotic condition

**Movie S6.** 3D MINFLUX example #1 of an ALFA-labelled and PIEZO1 expressing small neurite

**Movie S7.** 3D MINFLUX example #2 of an ALFA-labelled and PIEZO1 expressing small neurite